Proceedings of the Canadian Society for Mechanical Engineering International Congress
32nd Annual Conference of the Computational Fluid Dynamics Society of Canada
Canadian Society of Rheology Symposium
CSME-CFDSC-CSR 2025
May 25–28, 2025, Montréal, Québec, Canada

Comparative Study of the Discharge Architecture for a Multi-Energy Pumped Thermal Energy Storage System Using Finite Dimension Thermodynamics

Sullivan Durand[1*], Pierre Neveu[2], Daniel R. Rousse[1], Didier Haillot[1]
[1]Mechanical engineering department, École de Technologie Supérieure, Montréal, Canada
[2]University of Perpignan Via Domitia, Perpignan, France
*sullivan.durand.1@ens.etsmtl.ca

Abstract—This study presents a comparative assessment of the conventional discharge architecture of multi-energy Pumped Thermal Energy Storage (m-PTES) systems and an alternative configuration. In traditional architecture, the whole stored energy is devoted to supplying heat to the Rankine cycle which produces both electricity and useful thermal energy. On the contrary, in the alternative one, part of the stored energy is directly recovered through a heat exchanger to deliver thermal energy. The other part is used for the Rankine cycle. Thus, this cycle involves a lower capacity but it operates with the external environment as a heat sink. The performance of both configurations was analyzed using Finite Dimension Thermodynamics (FDT), considering key indicators such as power cycle efficiency, total required power, and heat exchanger conductances. This study uses the context of an industrial natural resource extraction process as a case study. The results show that the proposed configuration is more efficient when the external environment temperature is lower than the useful heat sink temperature. Additionally, this architecture achieves higher efficiencies for high power-to-heat ratios and storage temperatures below 497 °C. This research significantly contributes to the study of m-PTES systems by introducing a new discharge strategy, providing a detailed comparison with the conventional approach using FDT, and proposing heat exchanger optimization to minimize conductances.

Keywords – Energy storage; Multi-energy pumped thermal energy storage; Discharge cycle; Finite dimension thermodynamics

I. INTRODUCTION

The need to increase the share of renewable energy sources in the power grid goes hand in hand with the imperative to improve grid flexibility. Beyond demand management, expanding storage capacity is essential. To date, mechanical energy storage through pumped hydro storage has proven to be the most technically and economically efficient large-scale energy storage technology [1]. However, spatial and economic constraints significantly limit its deployment [2]. In response to the growing demand for low-cost electrical energy storage, attention has recently shifted toward alternative storage concepts such as Carnot batteries [3]. Among these, multi-energy Pumped Thermal Energy Storage (m-PTES) systems have emerged as a promising alternative [4].

Figure 1 illustrates the operating principle of m-PTES systems. These systems absorb electrical and thermal energy during a charging phase (integration), which is then stored in thermal form before being converted back into electrical and thermal energy during a discharge phase (restitution) [5]. The discharge process typically relies on a power cycle, most commonly a Rankine cycle. For charging, vapor compression cycles are commonly used [6]. The review of m-PTES systems in the scientific literature highlights a relatively uniform architecture, where thermal integration relies on directing waste heat to a heat exchanger that acts as an evaporator during the charging cycle. Heat recovery occurs at the exchanger corresponding to the condenser of the discharge cycle, enabling the reuse of rejected heat for other thermal applications. These systems offer three key advantages: (1) they help address the intermittency issues of renewable energy technologies; (2) they optimize the use of residual waste heat; and (3) they can provide temperature control for other processes.

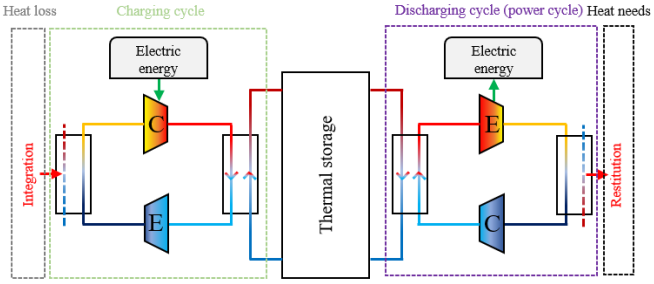

Figure 1. Operating principle and architecture of multi-energy PTES systems; C : compressor, E : expender.

Building on this architecture, Frate et al. [7] developed and simulated two m-PTES systems based on Organic Rankine Cycles. These systems were compared to lithium-ion batteries, which serve as a benchmark for residential energy storage. The results highlighted the superior performance of m-PTES systems compared to batteries. Similarly, Trebilcock et al. [8] examined an m-PTES system based on a Rankine cycle coupled with a district heating network, demonstrating the potential of this technology. The round-trip electrical efficiency, defined as the ratio of recovered electrical energy to supplied electrical energy over a charge/discharge cycle, is typically estimated at around 70%. However, some studies report values exceeding 100% due to the contribution of thermal integration [9].

The architecture presented in Figure 1 has a major limitation related to its thermal discharge process, which hinders both its efficiency and large-scale adoption. In its current form, thermal recovery can only occur during the system's discharge phase. This constraint reduces operational flexibility and may limit the system's potential in contexts where a stable thermal supply is essential, such as industrial processes. It is therefore necessary to develop an optimized discharge architecture that enables more flexible thermal recovery while minimizing economic and technical constraints.

The main objective of this study is to address the above-mentioned need and to evaluate its performance in comparison with the conventional architecture presented in Figure 1. This comparison will be conducted based on both energy and economic criteria. First, a new discharge architecture will be introduced. Then, this architecture will be compared to the conventional design using an analysis based on Finite Dimension Thermodynamics (FDT). The second part of this paper will focus on a detailed definition of the proposed discharge architecture, the modeling of both configurations—conventional and new—using FDT, and the selection of comparison criteria to assess their respective performance. The third part of this study will analyze the obtained results, highlighting the advantages and limitations of each configuration through the case study of an industrial resource industry. This analysis will assess potential energy efficiency gains as well as the economic implications of implementing the new architecture. Finally, the conclusion will summarize the key findings of the study.

II. ARCHITECTURE DEFINITION AND MODELING

This section provides a detailed description of the proposed discharge architecture, the modeling of both the conventional and alternative configurations using FDT, and the performance criteria used to compare their respective efficiencies.

A. *Proposal for the new discharge architecture*

As mentioned in the introduction, one of the main limitations of the currently employed discharge architecture is the inability to provide thermal recovery outside of the discharge phase. To overcome this constraint, one approach is to recover heat directly from the existing storage tank. This strategy involves integrating a network of heat exchangers positioned in parallel with the power block. Figure 2a illustrates the conventional discharge architecture (denoted A1), while Figure 2b presents the newly proposed configuration (denoted A2).

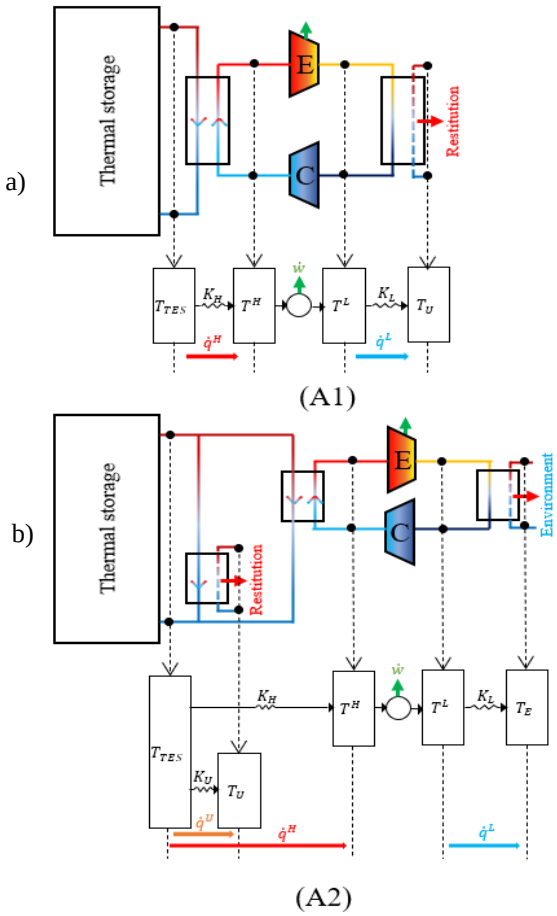

Figure 2. Conventional discharge architecture (a) and the proposed new configuration (b) and their equivalent models.

In the conventional architecture (A1), thermal recovery is provided by the heat flow released at the condenser of the power block. In contrast, in the proposed configuration (A2), this heat flow is directly dissipated to the external environment, while the thermal storage fluid becomes the primary heat source for the thermal recovery process. Although only one heat exchanger is illustrated here, integrating multiple exchangers in series remains feasible. This configuration offers several advantages, including more efficient management of the available heat. Furthermore, since the external environment is typically colder than the recovery environment, the discharge cycle efficiency is improved, thereby optimizing the use of stored energy.

B. *Modeling of the architectures in FDT*

FDT aims to overcome the assumption of reversible processes, which traditionally characterizes the Carnot cycle [10]. Its main objective is to design an initial system model, inspired by thermodynamics, to more realistically define the operational parameters of the system compared to a fully reversible configuration. In this study, FDT is used to analyze the operating parameters of each architecture, allowing for a subsequent comparison. The FDT formalism involves replacing the real components of the system with an equivalent thermodynamic system. The method, described by Neveu et al. [11], is briefly presented here for the heat exchangers and the power cycle.

Heat exchangers can be represented by a thermal conductance K, allowing a heat transfer rate $\dot{q}$ between two reservoirs at temperatures corresponding to the average entropic temperatures ($T = \Delta h/\Delta s$) of the hot and cold fluids. This heat flux can then be described simply by a Newton's law:

$$\dot{q} = \mathrm{K}(T_H - T_L) \tag{1}$$

For the power cycle, the same principle applies: a power cycle can be analyzed through an equivalent cycle operating between two reservoirs at temperatures T_H et T_L. In the case of Rankine cycles, these temperatures represent the average entropic temperatures of the working fluid as it passes through the evaporator and the condenser, respectively.

Equivalence models provide the ability to substitute any working fluid, for which temperature varies, with a thermal reservoir for which temperature corresponds to the previously defined average entropic temperature. Thus, all heat exchangers are modeled by a conductance, and each inlet/outlet point of the working fluid is replaced by a thermal reservoir. The equivalent models of architectures (A1) and (A2) are illustrated in Figure 2.

In the current architecture (Figure 2a), thermal storage at temperature T_{TES} transfers a heat flow $\dot{q}_H$ via a heat exchanger with conductance K_H. This flow is partially converted into work $\dot{w}$, while a residual heat flow $\dot{q}_L$ is dissipated through a heat exchanger with conductance K_L connected to a useful heat sink at temperature T_U. The required useful heat for the thermal recovery process, denoted $\dot{q}_U$, is thus less than or equal to $\dot{q}_L$. In the proposed configuration (Figure 2b), the thermal flow $\dot{q}_L$ is dissipated to a heat sink corresponding to the external environment at temperature T_E. In contrast, the useful heat $\dot{q}_U$ is directly extracted from the thermal storage and transferred to the useful heat sink at temperature T_U via a heat exchanger with conductance K_U.

Chambadal [12], Novikov [13] and Curzon and Ahlborn [14] demonstrated that, at the maximum power point (MPP), the power cycle efficiency reaches its maximum value, called the "nice radical efficiency" η_{MPP}. The operating parameters of the power cycle that allow this optimal efficiency to be achieved are then defined by [15] :

$$\eta = \frac{\dot{w}}{\dot{q}_H} = \eta_{MPP} = 1 - \sqrt{\frac{T_i}{T_{TES}}} \tag{2}$$

$$K_\Sigma = K_H + K_L = \frac{4\dot{w}}{\left(\sqrt{T_{TES}} - \sqrt{T_i}\right)^2} \tag{3}$$

$$K_H = K_L = \frac{K_\Sigma}{2} \tag{4}$$

$$T_H = \frac{\sqrt{T_{TES}} + \sqrt{T_i}}{2}\sqrt{T_{TES}} \tag{5}$$

$$T_L = \frac{\sqrt{T_{TES}} + \sqrt{T_i}}{2}\sqrt{T_i} \tag{6}$$

Where:

- $T_i = T_U$ for architecture (A1);
- $T_i = T_E$ for architecture (A2).

In architecture (A2), the conductance K_U is determined based on the useful heat flow $\dot{q}_U$ and the temperature of the useful heat sink T_U following Newton's law:

$$K_\mathrm{U} = \frac{\dot{q}_U}{T_{TES} - T_U} \tag{7}$$

C. Definition of comparison criteria

The energy and economic performance of each configuration depend on the total heat flow required to ensure the production of work $\dot{w}$ and thermal restitution $\dot{q}_U$, denoted $\dot{q}_{Tot}$, as well as the total sum of the conductances, denoted K_{Tot}.

From an energy perspective, architecture (A2) presents advantages over architecture (A1) if, for identical temperature parameters T_{TES}, T_U and identical electrical $\dot{w}$ and thermal $\dot{q}_U$ needs:

$$\eta^{A2} > \eta^{A1} \tag{8}$$

$$\dot{q}_{Tot}{}^{A2} = \dot{q}_H + \dot{q}_U < \dot{q}_{Tot}{}^{A1} = \dot{q}_H \tag{9}$$

Equation (8) implies that the heat power $\dot{q}_H$ required to achieve work production $\dot{w}$ is lower in architecture (A2) than in architecture (A1). Equation (9) shows that the total power required to meet the total needs, including both work production and thermal restitution $\dot{q}_U$, is lower in architecture (A2) than in architecture (A1).

From an economic perspective, architecture (A2) is more advantageous than architecture (A1) if, for identical temperatures T_{TES}, T_U, and work $\dot{w}$ and useful heat $\dot{q}_U$ needs, equation (9) is satisfied. This ensures a lower storage capacity for the same storage duration, leading to reduced costs for the storage tank. Since conductances are directly proportional to the heat exchange surface area, and thus to the cost of the heat exchangers, it follows that architecture (A2) is also more advantageous than architecture (A1) if:

$$K_{Tot}{}^{A2} = K_\Sigma + K_\mathrm{U} < K_{Tot}{}^{A1} = K_\Sigma \tag{10}$$

D. Comparison methodology

To establish a common basis for comparison, the case of an existing natural resource industry based in Canada was chosen [16]. In this industry, the average power demand $\dot{w}$ is 16.5 MW, while the average heat flow required $\dot{q}_U$ is 8.5 MW. The average annual temperature of the external environment T_E is -10 °C, and the heat sink is at a temperature T_U of 60°C, a typical value for heating networks.

The objective is to compare architectures (A1) and (A2) based on the power cycle efficiency (η), the total heat flow required ($\dot{q}_{Tot}$), and the total sum of the conductances (K_{Tot}), using the parameters mentioned above. The analysis variable is therefore the storage temperature T_{TES}. The minimum temperature is set to that of the useful heat sink T_U, while the maximum temperature is set to 1600°C, corresponding to the usability limit of liquid metals [17]. This temperature range allows for the evaluation of the impact of storage temperature on the performance of both configurations.

III. RESULTS ANALYSIS

This section presents the analysis of the results obtained from the maximum power point (MPP) sizing of architectures (A1) and (A2), using equations (2), (3), (7) and (9). The analysis is based on three main criteria: the power cycle efficiency (η), the total heat flow required ($\dot{q}_{Tot}$), and the total sum of the conductances (K_{Tot}). These results allow for comparing the performance of the two configurations based on the defined parameters.

A. Comparison of (A1) and (A2)

Figure 3 illustrates: a) the power cycle efficiency (η); b) the total heat flow required ($\dot{q}_{Tot}$), and c) the total sum of the conductances (K_{Tot}) for each of the two architectures (A1- continuous line and A2- dashed line), as a function of the storage temperature T_{TES}.

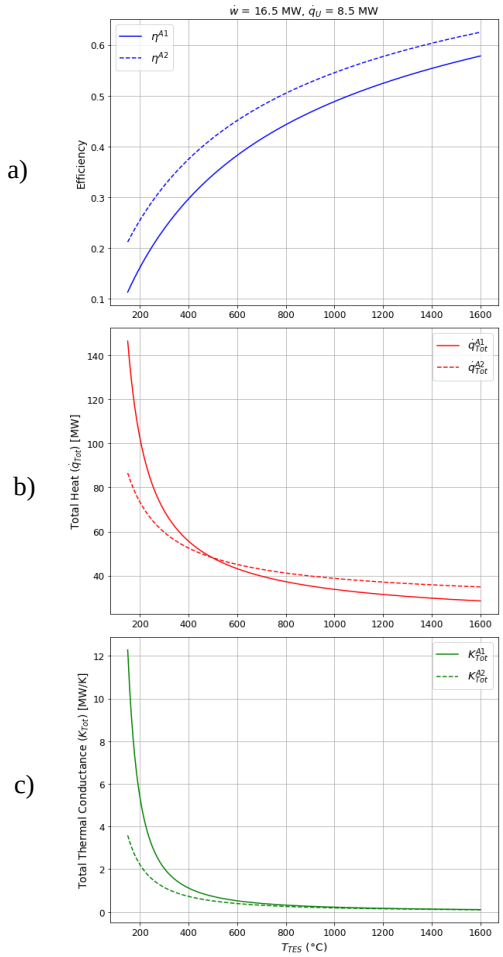

Figure 3. η, $\dot{q}_{Tot}$ et K_{Tot} for architectures (A1) and (A2) as a function of T_{TES}.

To begin, the power cycle efficiency of architecture (A2) (η^{A2}) is always higher than that of architecture (A1) (η^{A1}), regardless of the storage temperature T_{TES} (Figure 3a). This can be explained by equation (2), taking into account that $T_E < T_U$. Furthermore, logically, if $T_E > T_U$, architecture (A2) would become energetically and economically unfeasible compared to (A1), as the power cycle efficiency would be lower. Next, it is observed that for low storage temperatures (up to 497°C), ${\dot{q}_{Tot}}^{A2} < {\dot{q}_{Tot}}^{A1}$, and there is a storage temperature at which ${\dot{q}_{Tot}}^{A2} = {\dot{q}_{Tot}}^{A1}$ (Figure 4b). This storage temperature corresponds to the temperature T_{TES} where ${\dot{q}_H}^{A2} - {\dot{q}_H}^{A1} = \dot{q}_U$, meaning that the reduction in $\dot{q}_H$ in (A2), due to higher efficiency, is compensated by the thermal restitution $\dot{q}_U$. Finally, regarding the total sum of conductances, it is noted that ${K_{Tot}}^{A2} < {K_{Tot}}^{A1}$ for low storage temperatures, but ${K_{Tot}}^{A2}$ becomes nearly equal to ${K_{Tot}}^{A1}$ as T_{TES} increases (Figure 3c). Finally, as expected, the total heat flows $\dot{q}_{Tot}$ and the total conductances K_{Tot} decrease as the storage temperature increases.

From both an energetic and economic standpoint, (A2) is more advantageous than (A1) for low storage temperatures, up to around 497°C, as equations (8) to (10) are satisfied. At these temperatures, the power cycle efficiency and the management of $\dot{q}_U$ in (A2) allow for a reduction in the total heat flow required and the total conductance, making this architecture more cost-effective. However, beyond 497°C, architecture (A1) becomes more favorable, as the total power required to meet both thermal and electrical needs becomes lower in this configuration. Indeed, at high storage temperatures, architecture (A2) can no longer offer the same benefits in terms of reducing the required total heat power, which makes (A1) more competitive from both an energetic and economic perspectives.

B. Influence of the ratio $\dot{w}/\dot{q}_U$ on $\dot{q}_{Tot}$

An important point concerns the evolution of $\dot{q}_{Tot}$ as a function of $\dot{w}$, $\dot{q}_U$ et T_{TES}. Indeed, the total power required depends directly on the values of $\dot{w}$ and $\dot{q}_U$. Figure 4 shows the difference between ${\dot{q}_{Tot}}^{A1}$ and ${\dot{q}_{Tot}}^{A2}$ as a function of T_{TES} and the ratio $\dot{w}/\dot{q}_U$. In this analysis, $\dot{w}$ is kept constant (=16.5 MW), while $\dot{q}_U$ varies between 8.5 MW (reference value) and 16.5 MW. The reference situation corresponds to a ratio $\dot{w}/\dot{q}_U \approx 1.94$. This analysis allows for studying the impact of the ratio $\dot{w}/\dot{q}_U$ on the energy performance of the two architectures as a function of storage temperature.

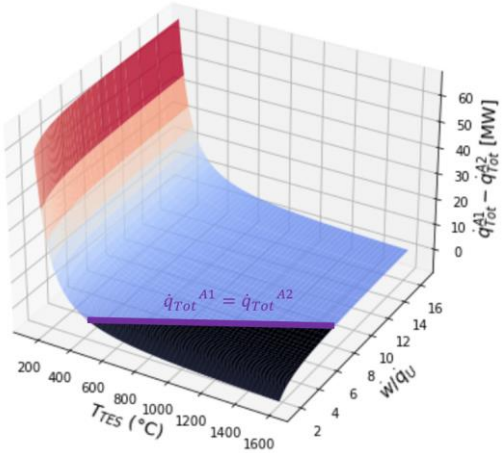

Figure 4. ${\dot{q}_{Tot}}^{A1} - {\dot{q}_{Tot}}^{A2}$ as a function of T_{TES} and $\dot{w}/\dot{q}_U$.

The dark area in Figure 4 corresponds to the set of points where $\dot{q}_{Tot}{}^{A1} - \dot{q}_{Tot}{}^{A2} < 0$. It thus represents the pairs $(\dot{w}/\dot{q}_U, T_{TES})$ for which the total heat power required in (A2) is greater than that in (A1). As can be observed, the proportion of combinations where $\dot{q}_{Tot}{}^{A2} < \dot{q}_{Tot}{}^{A1}$ is much higher than that for which $\dot{q}_{Tot}{}^{A2} > \dot{q}_{Tot}{}^{A1}$. More specifically, based on the total power criterion and considering the temperatures $T_U = 60$ °C and $T_E = -10$ °C, architecture (A1) is preferred to (A2) for $\dot{w}/\dot{q}_U \in [1.94, 7.69]$ and $T_{TES} > 497\,°C$. Notice that the increase in the environment temperature T_E would extend the dark surface area.

C. *Exchanger count influence on (A2) restitution*

Figure 3 showed that $K_{Tot}{}^{A2} < K_{Tot}{}^{A1}$ for low storage temperatures, but $K_{Tot}{}^{A2} \approx K_{Tot}{}^{A1}$ as T_{TES} increases. However, the (A2) configuration currently uses only a single heat exchanger with conductance K^{U} for thermal restitution (see Figure 3). In order to validate the performance of this configuration, it is relevant to study the effect of increasing the number of heat exchangers. Let n be the total number of heat exchangers in the thermal restitution in architecture (A2). The new equivalent model of (A2) is shown in Figure 5.

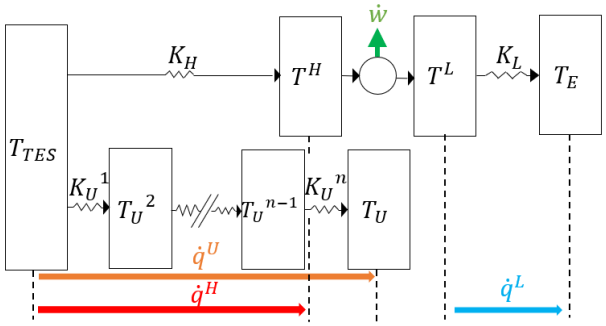

Figure 5. Equivalent model of architecture (A2) using n heat exchangers for thermal restitution.

Where:

- $K_U{}^i, \forall i \in [1 \dots n]$ corresponds to the heat exchanger conductances;
- $T_U{}^i, \forall i \in [1 \dots n+1]$ corresponds to intermediate temperatures.

The values of the conductances $K_U{}^i$ are determined by an optimization problem aimed at minimizing the total sum of the conductances, $K_{\mathrm{U}}{}^{\Sigma} = \sum_{i=1}^{n} K_U{}^i$. The solution to this problem is presented in the appendix. It is then demonstrated that:

$$K_{\Sigma}{}^U = \frac{n^2 \dot{q}_U}{T_{TES} - T_U}, \forall n \geq 1 \qquad (11)$$

Figure 6 shows the difference between $K_{Tot}{}^{A1}$ and $K_{Tot}{}^{A2}$ as a function of the storage temperature T_{TES} and the number of heat exchangers n. In this analysis, the reference values for T_U, $\dot{w}$ and $\dot{q}_U$ are kept constant.

It is clearly observed that increasing the number of heat exchangers in the thermal restitution process leads to a reduction in the storage temperature associated with $K_{Tot}{}^{A2} = K_{Tot}{}^{A1}$, which corresponds to the moment when (A1) becomes preferable to (A2) based on this criterion. For example, for $n = 2, T_{TES} \approx 1154\,°C$ and for $n = 5, T_{TES} \approx 310\,°C$. However, as T_{TES} increases, it is noted that $K_{Tot}{}^{A2}$ becomes equivalent to $K_{Tot}{}^{A1}$ again, regardless of the number of exchangers.

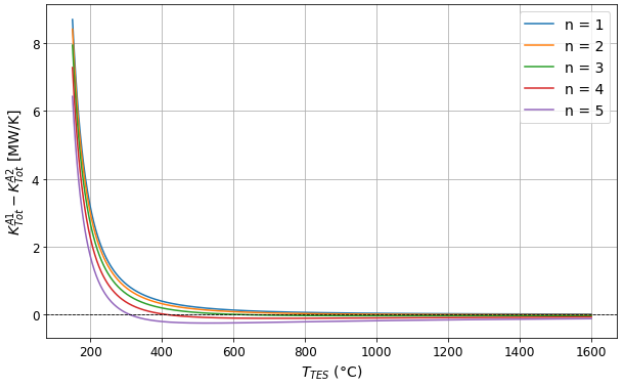

Figure 6. $K_{Tot}{}^{A1} - K_{Tot}{}^{A2}$ as a function of T_{TES} and n.

IV. Conclusion

The objective of this study was to compare, from an energy and economic perspective, the conventional discharge architecture of m-PTES systems, with a new configuration that allows for more flexible heat recovery. This new architecture is characterized by the use of the external environment as a heat sink for the power cycle and the direct utilization of the storage reservoir to supply useful heat to other processes. Both architectures were modeled using FDT and then compared based on efficiency criteria, total power required, and the total sum of heat exchanger conductances, with a natural resource industry as a case study. The system has an average power demand of 16.5 MW and a heat requirement of 8.5 MW, with an external temperature of -10°C and a heat sink at 60°C. The main results obtained are summarized below.

The proposed architecture has an energy and economic advantage only if $T_E > T_U$. In this context, the following results were observed:

- The power cycle efficiency of the proposed architecture is always higher than that of the conventional architecture.
- The difference in total power required to supply $\dot{w}$ and $\dot{q}_U$ depends on the storage temperature and the ratio of the two powers. When this power ratio is high, the proposed architecture performs better. However, for a low ratio and high storage temperatures, the conventional architecture becomes preferable.
- The higher the number of heat exchangers used for thermal discharge, the lower the storage temperature at which the total conductance sums become equal. For high storage temperatures, both configurations become equivalent in terms of this criterion.

For given values of T_E and T_U, the viability of one configuration over the other mainly depends on the total power required and the storage temperature. In the considered case study, and for storage temperatures below 497°C, the proposed configuration proves to be more advantageous.

ANNEXE

The optimization problem is formulated as follows:

$$min\left({K_U}^{\Sigma}\right) \quad (A1)$$

$${K_U}^{i}\left({T_U}^{i} - {T_U}^{i+1}\right) - \dot{q}_U = 0, \forall i \in [1 \dots n] \quad (A2)$$

$$\sum_{i=1}^{n} {K_U}^{i} - {K_U}^{\Sigma} = 0, \forall i \in [1 \dots n] \quad (A3)$$

$${T_U}^{1} = T_{TES} \; et \; {T_U}^{n+1} = T_U \quad (A4)$$

The storage temperature T_{TES}, the useful heat sink temperature T_U, and the useful heat required for the thermal recovery process $\dot{q}_U$ are parameters. The Lagrangian of the optimization problem is written as:

$$\mathcal{L}\left({K_U}^{i}, {K_U}^{\Sigma}, {T_U}^{i}, \lambda^{i}\right) = {K_U}^{\Sigma} + \sum_{i=1}^{n} {\lambda_A}^{i}\left[{K_U}^{i}\left({T_U}^{i} - {T_U}^{i+1}\right) - \dot{q}_U\right] + \lambda_B\left[\sum_{i=1}^{n} {K_U}^{i} - {K_U}^{\Sigma}\right] \quad (A5)$$

With λ^i being the Lagrange multipliers. The optimal conditions are:

$$\frac{\partial \mathcal{L}}{\partial {K_U}^{i}} = {\lambda_A}^{i}\left({T_U}^{i} - {T_U}^{i+1}\right) + \lambda_B = 0, \forall i \in [2 \dots n] \quad (A6)$$

$$\frac{\partial \mathcal{L}}{\partial {K_U}^{\Sigma}} = 1 - \lambda_B = 0 \quad (A7)$$

$$\frac{\partial \mathcal{L}}{\partial {T_U}^{i}} = {\lambda_A}^{i}{K_U}^{i} - {\lambda_A}^{i-1}{K_U}^{i-1} = 0, \forall i \in [2 \dots n] \quad (A8)$$

$${K_U}^{i}\left({T_U}^{i} - {T_U}^{i+1}\right) - \dot{q}_U = 0, \forall i \in [1 \dots n] \quad (A9)$$

$$\sum_{i=1}^{n} {K_U}^{i} - {K_U}^{\Sigma} = 0, \forall i \in [1 \dots n] \quad (A10)$$

$${T_U}^{1} = T_{TES} \; et \; {T_U}^{n+1} = T_U \quad (A11)$$

From equation (A7): $\lambda_B = 1$. It is then possible to express ${\lambda_A}^{i}$ using (A6) and then ${\lambda_A}^{i-1}$ by changing the index. By substituting these into (A8):

$${K_U}^{i} = {K_U}^{i-1}\frac{{T_U}^{i} - {T_U}^{i+1}}{{T_U}^{i-1} - {T_U}^{i}} \quad (A12)$$

By expressing ${K_U}^{i}$ using (A9), ${K_U}^{i-1}$ through an index change, and substituting them into (A12):

$${T_U}^{i} = \frac{{T_U}^{i-1} + {T_U}^{i+1}}{2}, \forall i \in [2 \dots n] \quad (A13)$$

This is an arithmetic sequence with the first term ${T_U}^{1} = T_{TES}$ and the last term ${T_U}^{n+1} = T_U$. In this case:

$${T_U}^{i} = T_{TES} + \; (i-1)\frac{T_U - T_{TES}}{n}, \forall n \geq 1 \quad (A14)$$

By expressing ${T_U}^{i+1}$ through an index change and introducing (A14) and ${T_U}^{i+1}$ in (A9):

$${K_U}^{i} = \frac{n\dot{q}_U}{T_{TES} - T_U}, \forall n \geq 1 \quad (A15)$$

This demonstrates the equality of all the conductances. Finally, (A10) implies:

$${K_U}^{\Sigma} = \sum_{i=1}^{n} {K_U}^{i} = \frac{n^2\dot{q}_U}{T_{TES} - T_U}, \forall n \geq 1 \quad (A16)$$

REFERENCES

[1] P. C. Nikolaos, F. Marios, and K. Dimitris, "A Review of Pumped Hydro Storage Systems," *Energies*, vol. 16, no. 11, Art. no. 11, Jan. 2023, doi: 10.3390/en16114516.

[2] M. Gimeno-Gutiérrez and R. Lacal-Arántegui, "Assessment of the European potential for pumped hydropower energy storage based on two existing reservoirs," *Renewable Energy*, vol. 75, pp. 856–868, Mar. 2015, doi: 10.1016/j.renene.2014.10.068.

[3] A. Benato and A. Stoppato, "Pumped Thermal Electricity Storage: A technology overview," *Thermal Science and Engineering Progress*, vol. 6, pp. 301–315, Jun. 2018, doi: 10.1016/j.tsep.2018.01.017.

[4] A. Ghilardi, G. Frate, K. G. Kyprianidis, M. Tucci, and L. Ferrari, "Multi-Energy Brayton Pumped Thermal Energy Storage: A Milp Approach for Optimal Energy Dispatchment in a Multi-Energy District," Feb. 29, 2024, *Rochester, NY*: 4743196. doi: 10.2139/ssrn.4743196.

[5] S. Sharma and M. Mortazavi, "Pumped thermal energy storage: A review," *International Journal of Heat and Mass Transfer*, vol. 213, p. 124286, Oct. 2023, doi: 10.1016/j.ijheatmasstransfer.2023.124286.

[6] O. Dumont, G. F. Frate, A. Pillai, S. Lecompte, M. De paepe, and V. Lemort, "Carnot battery technology: A state-of-the-art review," *Journal of Energy Storage*, vol. 32, p. 101756, Dec. 2020, doi: 10.1016/j.est.2020.101756.

[7] G. F. Frate, L. Ferrari, P. Sdringola, U. Desideri, and A. Sciacovelli, "Thermally integrated pumped thermal energy storage for multi-energy districts: Integrated modelling, assessment and comparison with batteries," *Journal of Energy Storage*, vol. 61, p. 106734, May 2023, doi: 10.1016/j.est.2023.106734.

[8] Trebilcock, F., Ramirez., Pascual, C., Weller, T., Lecompte, S., and Hassan A. H, "Development of a compressed heat energy storage system prototype.," *IIR Rankine Conference 2020*. Jul. 2020. doi: 10.18462/iir.rankine.2020.1178.

[9] O. Dumont and V. Lemort, "Mapping of performance of pumped thermal energy storage (Carnot battery) using waste heat recovery," *Energy*, vol. 211, p. 118963, Nov. 2020, doi: 10.1016/j.energy.2020.118963.

[10] P. Neveu, B. Rebouillat, and Q. Falcoz, "Finite Dimension Thermodynamics for Optimizing Power Plants Including Heat Storage Device," in *Proceedings of ECOS 2023 - the 36th international conference on efficiency, cost, optimization, simulation and environmental impact of energy systems*, LAS PALMAS DE GRAN CANARIA,, Spain: ECOS 2023, Jun. 2023, pp. 136–147. doi: 10.52202/069564-0014.

[11] P. Neveu, F. Ayachi, C. Leray, and Y. Azoumah, "Optimal integration of rankine cycles in concentrated sol power plant," presented at the ECOS 2015 - 28th International Conference on Efficiency, Cost, Optimization, Simulation and Environmental Impact of Energy Systems, 2015.

[12] P. Chambadal, *Les centrales nucléaires*, Armand Colin. Paris, 1957.

[13] I. I. Novikov, "The efficiency of atomic power stations (a review)," *Journal of Nuclear Energy (1954)*, vol. 7, no. 1, pp. 125–128, Aug. 1958, doi: 10.1016/0891-3919(58)90244-4.

[14] F. L. Curzon and B. Ahlborn, "Efficiency of a Carnot engine at maximum power output," *American Journal of Physics*, vol. 43, pp. 22–24, Jan. 1975, doi: 10.1119/1.10023.

[15] B. Rebouillat, "Conception et Intégration optimales des convertisseurs thermodynamiques d'énergie solaire concentrée," 2021.

[16] A. Robert, "Conception d'un stockage d'énergie éolienne pour une entreprise minière isolée du réseau : faisabilité du stockage par batteries à flux," Master's Thesis, École de technologie supérieure, 2023. Accessed: Oct. 30, 2023. [Online]. Available: https://espace.etsmtl.ca/id/eprint/3230/

[17] G. Alva, Y. Lin, and G. Fang, "An overview of thermal energy storage systems," *Energy*, vol. 144, pp. 341–378, Feb. 2018, doi: 10.1016/j.energy.2017.12.037.